RESEARCH ARTICLE

Key Points:
- The CRTM is modified to use microwave scattering look-up tables made consistent with cloud/precipitation properties of microphysics schemes
- The CRTM as-released, using effective radius to specify cloud particle sizes, produces higher brightness temperatures than the modified CRTM
- Brightness temperatures are sensitive to the assumed bulk density of graupel and ice cloud particle sizes produced by microphysics schemes

Correspondence to:
F. Zhang,
fzhang@psu.edu

Comparison of using distribution-specific versus effective radius methods for hydrometeor single-scattering properties for all-sky microwave satellite radiance simulations with different microphysics parameterization schemes

Scott B. Sieron[1] iD, **Eugene E. Clothiaux[1]** iD, **Fuqing Zhang[1]** iD, **Yinghui Lu[1]** iD, **and Jason A. Otkin[2]** iD

[1]Department of Meteorology and Atmospheric Science, and Center for Advanced Data Assimilation and Predictability Techniques, Pennsylvania State University, University Park, Pennsylvania, USA, [2]Cooperative Institute for Meteorological Satellite Studies, Space Science and Engineering Center, University of Wisconsin-Madison, Madison, Wisconsin, USA

Abstract The Community Radiative Transfer Model (CRTM) presently uses one look-up table (LUT) of cloud and precipitation single-scattering properties at microwave frequencies, with which any particle size distribution may interface via effective radius. This may produce scattering properties insufficiently representative of the model output if the microphysics parameterization scheme particle size distribution mismatches that assumed in constructing the LUT, such as one being exponential and the other monodisperse, or assuming different particle bulk densities. The CRTM also assigns a 5 μm effective radius to all nonprecipitating clouds, an additional inconsistency. Brightness temperatures are calculated from 3 h convection-permitting simulations of Hurricane Karl (2010) by the Weather Research and Forecasting model; each simulation uses one of three different microphysics schemes. For each microphysics scheme, a consistent cloud scattering LUT is constructed; the use of these LUTs produces differences in brightness temperature fields that would be better for analyzing and constraining microphysics schemes than using the CRTM LUT as-released. Other LUTs are constructed which contain one of the known microphysics inconsistencies with the CRTM LUT as-released, such as the bulk density of graupel, but are otherwise microphysics-consistent; differences in brightness temperature to using an entirely microphysics-consistent LUT further indicate the significance of that inconsistency. The CRTM LUT as-released produces higher brightness temperature than using microphysics-consistent LUTs. None of the LUTs can produce brightness temperatures that can match well to observations at all frequencies, which is likely due in part to the use of spherical particle scattering.

1. Introduction

Satellite-borne passive microwave radiometers provide observations rich in meteorological information. Collections of frequencies close to maximum absorption and emission by oxygen and water vapor, called atmospheric sounding channels, are informative of the vertical profile of temperature and moisture, respectively; assimilation of these observations have been among the most impactful in reducing errors in global forecasts [e.g., *Zhu and Gelaro*, 2008]. Imaging channels occur at frequencies away from those with strong absorption and emission by gases. Measurements at these frequencies are more informative of the surface and hydrometeors, providing information on the integrated mass, phase, and particle sizes in clouds and precipitation. There is growing interest in passive microwave observations for direct assimilation in numerical weather prediction (NWP) at regional [e.g., *Zhang et al.*, 2013; *Shen and Min*, 2015; *Bao et al.*, 2015] and global scales [e.g., *Kazumori et al.*, 2016; *Zhu et al.*, 2012; *Geer and Bauer*, 2011], and signal-based NWP model evaluation [e.g., *Wiedner et al.*, 2004; *Meirold-Mautner et al.*, 2007; *Matsui et al.*, 2009; *Han et al.*, 2013; *Hashino et al.*, 2013].

These applications of satellite brightness temperature observations require a radiative transfer model as (at least) a forward/observation operator to calculate the radiance produced by the simulated atmospheric state variables, including hydrometer species, from a NWP model. The Community Radiative Transfer Model (CRTM) [*Han et al.*, 2006], a product of the Joint Center for Satellite Data Assimilation, is a one-dimensional plane-parallel homogeneous radiative transfer solver with tangent-linear and adjoint models. In the CRTM, an instance of a specific hydrometeor species is specified by the atmospheric layer(s) in which it is located, its water content (kilograms per square meter of atmosphere), and for precipitation species—rain, snow,

Table 1. Scattering Optical Depths and Brightness Temperatures Output From CRTM Simulations With the Same Water Content, Effective Radius, and Particle Properties but With Different Particle Size Distributions[a]

Effective Radius (microns)	Water Content (g m^{-3})	Monodisperse		Exponential	
		Scattering Optical Depth	Brightness Temperature (K)	Scattering Optical Depth	Brightness Temperature (K)
0	0	0	276.18	0	276.18
103.7	1.15×10^{-4}	4.03×10^{-6}	272.96	1.74×10^{-5}	272.96
184.3	1.15×10^{-3}	2.24×10^{-4}	272.91	8.79×10^{-4}	272.79
327.8	1.15×10^{-2}	1.21×10^{-2}	270.57	3.49×10^{-2}	267.94
582.9	1.15×10^{-1}	5.54×10^{-1}	204.09	$1.00 \times 10^{+0}$	200.35
1037	$1.15 \times 10^{+0}$	$1.16 \times 10^{+1}$	75.57	$2.05 \times 10^{+1}$	74.74

[a]The CRTM is configured to simulate the 91.665 GHz horizontal polarization channel of the SSMIS aboard satellite DCSP-16. The particle used is an ice sphere with bulk density 500 kg m^{-3}. The exponential particle size distribution is for WSM6 graupel, for which the intercept parameter $N_0[\text{m}^{-3} \text{ m}^{-1}] = 4.0 \times 10^6$. The specified water content is applied to every level with temperature less than 263.15 K and pressure greater than 50 hPA (roughly 7.5 km to 20 km) and is the only cloud or precipitation in the CRTM profile. The other attributes of the profile (temperature, pressure) were taken from the outer region of a tropical cyclone in a WRF simulation, and the surface is ocean.

graupel, and hail—the effective radius of the comprising collection of hydrometeors. The specific (per-mass) absorption and scattering properties of the various hydrometeor species are contained in look-up tables (LUTs) having microwave frequency, effective radius, and, for liquid species, temperature as its dimensions. The precipitation species differ from each other either in phase (e.g., rain is liquid) or particle bulk density.

Implicit to the CRTM as-released is that particular size distributions of particles of the specified bulk density, with associated values of effective radius, were used in calculating the single-scattering property values in the LUT. However, neither the CRTM support literature nor source code specifies what particle size distributions were used.

It is also not specified how the effective radius, r_{eff}, relates to these particle size distributions. However, the definition of effective radius accepted by the radiative transfer community is the ratio of the third and second moments of the particle size distribution, N:

$$r_{\text{eff}} = \frac{\int r^3 N(r) dr}{\int r^2 N(r) dr}.$$

The derivation of this effective radius definition can be found in *Hansen and Travis* [1974]. Effective radius is conceptualized as the "mean radius for scattering," and the relationship between particle size and magnitude of scattering (i.e., scattering cross section) is taken to be related to the physical cross-sectional area of the particle. This relationship is a simple yet generally valid description for particles much larger than the wavelength of the radiation, i.e., in the geometric optics limit. At the opposite extreme—particles of maximum dimension much smaller than the wavelength—the magnitude of scattering relates to the square of the particle mass, i.e., in the Rayleigh scattering regime.

For distributions of either cloud or precipitation particles, the geometrical optics limit for scattering is not entirely appropriate for any microwave wavelength. The most commonly used satellite-borne passive microwave radiometer wavelengths for meteorological purposes range from 30 mm to 1.5 mm, or frequencies 10 GHz to 200 GHz. Small precipitation particles and most cloud particles are much smaller than these wavelengths, while the sizes of the larger hydrometeors are close to, perhaps greater than, these wavelengths. Under these circumstances, effective radius—or any method of interfacing to a single LUT—is likely *ineffective* at its supposed intent of correctly predicting the magnitude of scattering universally for all kinds of cloud and precipitation particle size distributions.

Consider the results of CRTM simulations in Table 1 in which different size distributions of ice spheres of identical bulk density with identical total water content and effective radius produce significantly different scattering optical depths and some differences in brightness temperature. Similar circumstances exist for ice cloud particles and infrared radiation; *Baran et al.* [2014, 2016] have demonstrated improvement in

modeled shortwave and longwave fluxes by directly coupling particle size distributions to scattering properties instead of parameterizing this relationship via effective radius.

For data assimilation and model evaluation, particle size distributions of interest are those used by a microphysics scheme within a NWP model. Microphysics schemes are used to describe the movement of atmospheric water between vapor and various species of clouds and precipitation. A bulk microphysics parameterization scheme will use a fixed form of particle size distribution for each species and predict one or more moments of the distribution. Different microphysics schemes make different assumptions on the particle properties and size distributions or predict different quantities of the distribution. These differences between schemes can cause instances of the same species label (e.g., "graupel") to have the same water content, or even the same effective radius, but different size distributions and scattering properties.

If certain assumptions on the size distributions and particle properties, e.g., form of the particle size distribution or particle bulk density, made by a microphysics scheme do not match those used in constructing the CRTM scattering property LUT, then the CRTM would incorrectly express the scattering properties of the clouds and precipitation produced by that microphysics scheme. While much is not known about the scattering property LUT in the current CRTM (version 2.1.3), there are some known inconsistencies between it and the microphysics schemes used in this study. Two inconsistencies relate to the lack of universality of a single LUT: the bulk density of graupel in the current CRTM is inconsistent with one scheme, and two schemes use a monodisperse distribution for the liquid and ice cloud species, while the third scheme uses gamma and exponential, respectively. (The single LUT in the current CRTM is assuredly inconsistent with at least one or the other of these schemes.) The nature of the latter of these two inconsistencies—exponential versus monodisperse particle size distribution—is not investigated beyond the experiment for producing Table 1. Instead, we investigate a known inconsistency between the current CRTM and all three microphysics schemes: the CRTM fixes ice cloud effective radii at 5 μm.

We modified the forward model of the CRTM (version 2.1.3) such that the single-scattering properties of hydrometeor species are exactly consistent with the particle size distributions and particle properties as specified by a microphysics parameterization scheme. Results of simulations using three microphysics schemes implemented in the Weather Research and Forecasting (WRF) model [*Skamarock et al.*, 2008] are presented. The development of the primary method, "Distribution-Specific," for implementing microphysics scheme consistency is outlined in section 2. Section 3 describes the case study for testing the concept. Results from both the unmodified and modified CRTM are analyzed in section 4. In section 5, we discuss the suitability of the unmodified and distribution specific CRTM for different applications, and possible future advancements in specifying cloud scattering properties.

2. Methodology

To obtain cloud and precipitation single-scattering properties that are consistent with a given particle size distribution and set of properties (i.e., ice bulk densities and liquid temperatures), one must integrate the single-scattering properties over the particle size distribution. To date, we have created support for the following microphysics parameterization schemes available in WRF model version 3.6.1 [*Skamarock et al.*, 2008]: WRF Single-Moment 6-Class (WSM6) [*Dudhia et al.*, 2008], Goddard (single-moment [*Lang et al.*, 2007]), and Morrison (double-moment [*Morrison et al.*, 2009]).

2.1. Microphysics Scheme Details

We identified the underlying parametric representation, and any explicit value ranges of the parameters, for the number, sizes, and bulk densities of particles for each microphysics scheme.

The precipitation species in WSM6 and Goddard have a gamma particle size distribution with a shape parameter 0, also called an exponential particle size distribution:

$$N(D) = N_0 e^{-\lambda D}.$$

The intercept parameter is N_0, and the slope parameter is $\lambda [m^{-1}] = \left(\frac{\pi \rho N_0}{\rho_a q} \right)^{1/4}$, where ρ is the particle density, ρ_a is the air density, and q is the mass mixing ratio ($\rho_a q$ is water content, mass of hydrometeor per volume

of air). Particle (bulk) density varies with the ice species; e.g., graupel has a higher density than snow. With the particle density and intercept parameter set constant, the scattering and absorption coefficients for the species depend only on the water content; however, snow in WSM6 also has a temperature-dependent intercept parameter.

In the Morrison scheme (as implemented in this study), all species but cloud water have two moments of an exponential particle size distribution (with $\lambda[\text{m}^{-1}] = \left(\frac{\pi \rho N}{q}\right)^{1/3}$ and $N_0[\text{kg}^{-1}\text{m}^{-1}] = N\lambda$) predicted: mass mixing ratio, q, and number concentration, N. Both variables impact the scattering properties of a given instance of the species.

The monodisperse cloud species come in greater variety of parametric representations, from having a fixed particle size (e.g., liquid cloud in Goddard), to having the particle size, number concentration, and sphere-equivalent bulk density all vary with water content (e.g., ice cloud in WSM6).

Except for ice cloud in WSM6, the size distributions of all hydrometeor species imply that the particles have a ratio of mass, M, to diameter, D, consistent with a sphere, that is, $M \propto \rho D^3$. See Appendix A for additional details on the specifications of the microphysics schemes used in this study, including cloud water in Morrison.

2.2. Particle Scattering Properties

Building microphysics-scheme consistent cloud single-scattering properties requires integration of individual particle scattering properties over the specified size distributions. The CRTM single-scattering look-up table (LUT) as released only provides properties averaged over (unknown) particle size distributions, not of individual particles. Furthermore, there is no information provided on the source or method for computing scattering properties contained in the CRTM LUT. Therefore, an independent source of particle single-scattering properties is required to construct single-scattering properties consistent with the microphysics schemes.

All species of the three microphysics schemes that we investigated (except for cloud ice in WSM6) have a particle size distribution formulated using a spherical particle mass-size relationship and provide no information on particle inhomogeneity. In order to be consistent with both the particle size distribution and the mass distribution of the species as specified by the microphysics scheme, the particles used in calculating scattering properties need to be spheres as well. Additionally, consistency with the CRTM LUT as-released in this matter is desirable when comparing brightness temperatures, and it was presumably created using spheres: it is likely to have been created at least several years ago, and it specifies a single particle bulk density for each ice species. We calculated the single-scattering properties of these spheres using a code based on Mie theory [*Bohren and Huffman*, 1983] and used the Maxwell-Garnett mixing formula to estimate the dielectric constant of ice with different bulk densities, treating ice as the inclusion and air as the matrix. The suitability of Mie theory and spherical-particle scattering in this application is discussed in section 5.

At each of 38 microwave frequencies (matching the frequencies used in the CRTM LUT), we calculated single-scattering properties for sphere diameters ranging from 2 μm to 20000 μm in steps of 2 μm. For the liquid species, we repeated these calculations with particle temperatures ranging from 263.16 K to 303.16 K in 10 K steps (again matching the CRTM microwave LUT) to account for variation in dielectric constant [*Turner et al.*, 2016]. One temperature (273.15 K) for ice scattering calculations is sufficient for the database in this study because the CRTM as-released has temperature-independent microwave scattering LUT for ice species. For the ice spheres, we repeated these calculations with bulk densities ranging from 1 kg m^{-3} to 920 kg m^{-3} in 1 kg m^{-3} steps. (WSM6 specifies ice cloud particles to have continually varying sphere-equivalent bulk density with water content.) In addition to calculating scattering and absorption cross sections, $\sigma_s(D)$ and $\sigma_a(D)$, and asymmetry parameters, $g(D)$, we used the Mie computations to calculate the scattering phase function at 0.1° resolution, which is then decomposed into a smaller set of Legendre polynomial coefficients.

2.3. Cloud Scattering Properties for CRTM Distribution-Specific

After obtaining the prerequisite microphysics scheme information and sphere scattering data, the microphysics scheme particle property and size distribution information were applied in the construction of hydrometeor species single-scattering property LUTs. First, we created a parameter space of the hydrometeor
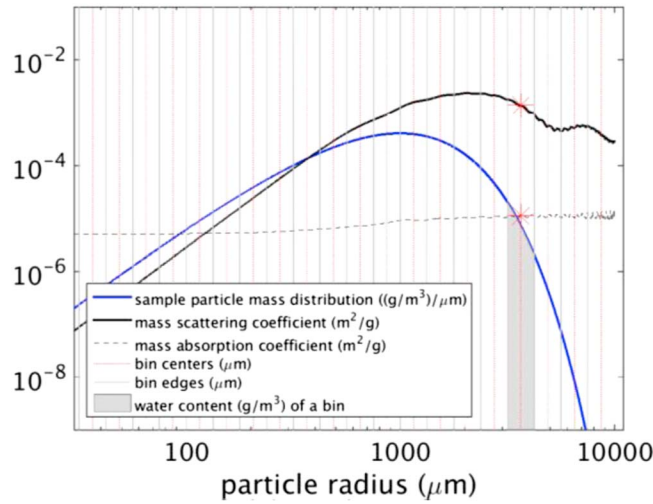
Figure 1. A sample relationship between mass scattering coefficients, mass absorption coefficients, and particle mass distribution, and a sample discretization for integration. Mass scattering and absorption coefficients are for ice spheres of bulk density 500 kg m^{-3} at 91.665 GHz; particle mass distribution is for WSM6 graupel with water content 1.24 g m^{-3}. The locations of bin edges and centers are for 32 bins spaced logarithmically. The grey shading beneath the particle mass distribution and between two adjacent bin edges represents the mass per unit volume of the corresponding bin. The red stars along the bin center at the mass scattering and absorption coefficient lines represent the values of these quantities applicable for the bin.

properties (water content and particle number concentration) and atmospheric properties (temperature) relevant to the scattering and absorption properties of each species of each microphysics scheme. (Bulk density is also relevant to single-scattering properties but is either fixed or entirely dependent on water content.) We determined lower and upper bounds for each parameter and discretized the parameter space. At each location in the parameter space of a species, we calculated single-scattering properties of the specified by integrating across the specified particle size distribution, $N(D)$. The scattering and absorption cross sections, $\sigma_s(D)$ and $\sigma_a(D)$, and asymmetry parameters, $g(D)$, of the specified particle properties are used to calculate scattering and absorption coefficients,

$$\beta_s = \int_0^\infty \sigma_s(D)N(D)dD,$$

$$\beta_a = \int_0^\infty \sigma_a(D)N(D)dD,$$

and cloud asymmetry parameter,

$$g = \frac{1}{\beta_s}\int_0^\infty g(D)\sigma_s(D)N(D)dD.$$

Similarly, the scattering phase function Legendre polynomial coefficients are computed from individual particle results:

$$L_N = \frac{1}{\beta_s}\int_0^\infty L_N(D)\sigma_s(D)N(D)dD,$$

where L_N is the Legendre order index N. In this application, the numerical integration was truncated to spheres of diameters of 2 μm to 20,000 μm, and discretized by 2 μm. Figure 1 graphically demonstrates this numerical integration process, though at much lower resolution than the 2 μm diameter spacing used here. This numerical integration was repeated for each microwave frequency and for each of the five liquid temperatures.

For each microphysics scheme, the LUTs of all species were compiled into a binary file for use by the CRTM. Additionally, the CRTM LUTs contain extension coefficients and single-scattering albedos instead of scattering and absorption coefficients. Modifications to the CRTM were required to support the new LUTs due to the addition and removal of certain variables as dimensions.
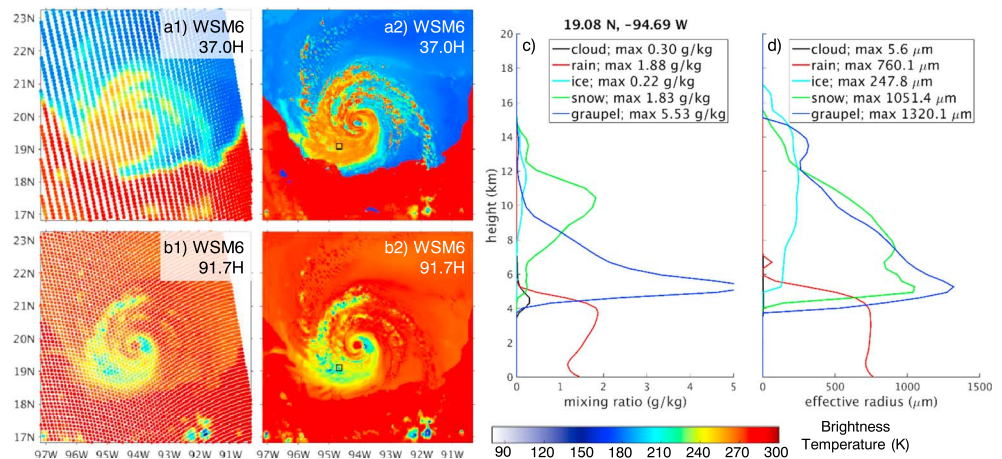
Figure 2. CRTM-RE simulations (a1 and b1) after (approximate) satellite beam convolution and (a2 and b2) at native WRF resolution. (c and d) The vertical profiles of mixing ratio and effective radius at the location centered in the small black box overlaying Figures 2a2 and 2b2.

The procedural changes for using the modified CRTM were to specify cloud mass by mixing ratio (instead of water content), the depths (meters) of atmospheric layers, the cloud number concentration for instances of double-moment species, and, of course, to not specify cloud effective radius. Mixing ratio was chosen as the mass variable for convenience to the user because it is the microphysics variable contained in the WRF output files. The depth of layers is necessary—along with air density, which is calculated by the modified CRTM—to convert mixing ratio into layer water content for the hydrometeor radiative property calculations.

We refer to this implementation of CRTM with microphysics-consistent radiative properties as CRTM Distribution-Specific (CRTM-DS). The standard CRTM with hydrometeor single-scattering properties based on effective radius will be referred to as CRTM-RE.

3. Test Case

We applied both CRTM-RE and CRTM-DS to the output of Weather Research and Forecasting (WRF) simulations. Hurricane Karl (2010) simulations were initialized at 21 UTC on 16 September from an EnKF analysis assimilating airborne Doppler radar observations as presented in *Melhauser et al.* [2017] following the methodologies developed in *Zhang and Weng* [2015] and *Weng and Zhang* [2012]. The WRF simulations differed only in microphysics scheme: WSM6, Goddard, or Morrison. These simulations used four two-nested domains with grid spacing of 27 km, 9 km, 3 km, and 1 km; here, we consider only the 3 h forecast (valid at 00 UTC on 17 September) for the 3 km domain.

For this study, the CRTM is configured to simulate the Special Sensor Microwave Imager/Sounder (SSMIS) aboard satellite Defense Meteorological Satellite Program (DMSP)-16 with a view zenith angle set to 53.1°. The FAST microwave Emissivity Model version 5 (FASTEM5) sea surface emissivity model is used, along with the Successive Order of Interaction solver [*Greenwald et al.*, 2004], which yielded comparable results to the Advanced Double Adding solver [*Liu and Weng*, 2006]. Because built-in estimation of the appropriate number of streams in the CRTM is based on the effective radius, a quantity which CRTM-DS does not use, we set the CRTM to use 16 + 2 streams for all profiles.

The CRTM was run at the native WRF 3 km resolution, and the brightness temperatures were mapped to the locations of F16 SSMIS observations of Hurricane Karl valid at 0117 UTC on 17 September. This mapping approximated satellite beam convolution, as we calculated a weighted mean of the CRTM simulated brightness temperatures near the observation location using the average of the cross- and along-track effective fields of view as the −3 dB width (1.18σ) of a two-dimensional Gaussian weighting function [*Bennartz*, 2000]. Figure 2 contains plots of mapped brightness temperatures adjacent to plots of brightness temperatures at the native WRF grid spacing (3 km) for comparison.
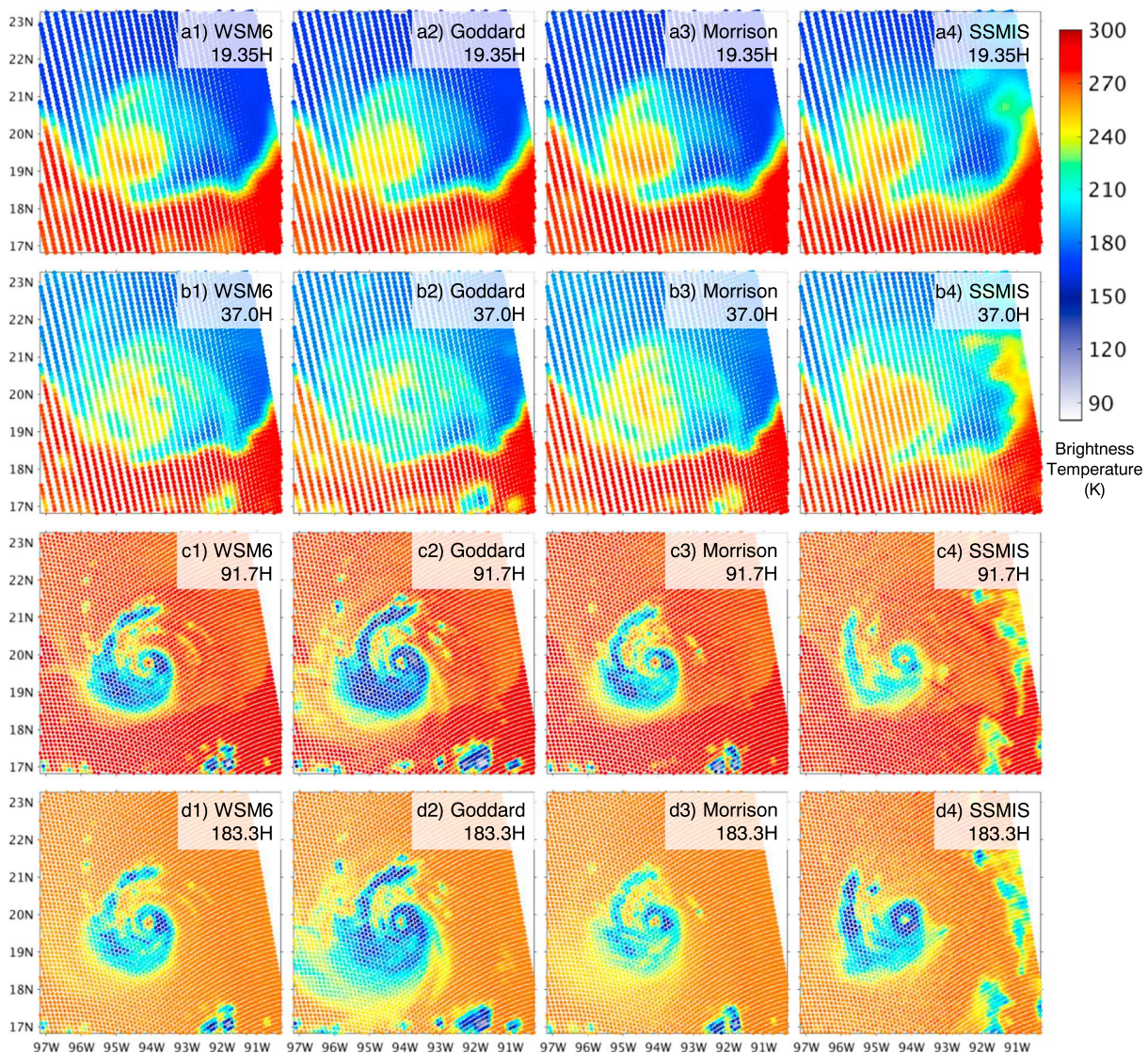
Figure 3. (columns 1–3) Outputs of CRTM-DS (microphysics-consistent hydrometeor scattering properties) from WRF simulations and (column 4) SSMIS observations of Hurricane Karl valid at 0000 UTC and 0117 UTC, respectively, on 17 September. The microphysics schemes used in the WRF simulations are (1) WSM6, (2) Goddard, and (3) Morrison.

Summary statistics for different CRTM simulations were calculated in a smaller area than the entire domain, chosen to contain the primary cloud and precipitation shield of the hurricane and exclude much of the area with clear air, the far outer rainbands of the hurricane, and convection unrelated to the hurricane. This area is enclosed by 18.0°N to 21.5°N and 96.0°W to 92.5°W.

4. Results

4.1. CRTM-DS and CRTM-RE

The brightness temperatures from using the CRTM with microphysics-consistent radiative properties (CRTM-DS) are illustrated in Figure 3, while those obtained from CRTM-RE are illustrated in Figure 4. These and other figures with a focus on simulated brightness temperatures also include plots of F16 SSMIS observations of the hurricane valid at 0117 UTC on 17 September, which are provided to indicate the fidelity of the simulations. Table 2 (upper half) contains average errors of CRTM-RE brightness temperatures relative to the CRTM-DS simulation. Comparison of simulated brightness temperatures to observations (lower half of Table 2) is reserved for the discussion.
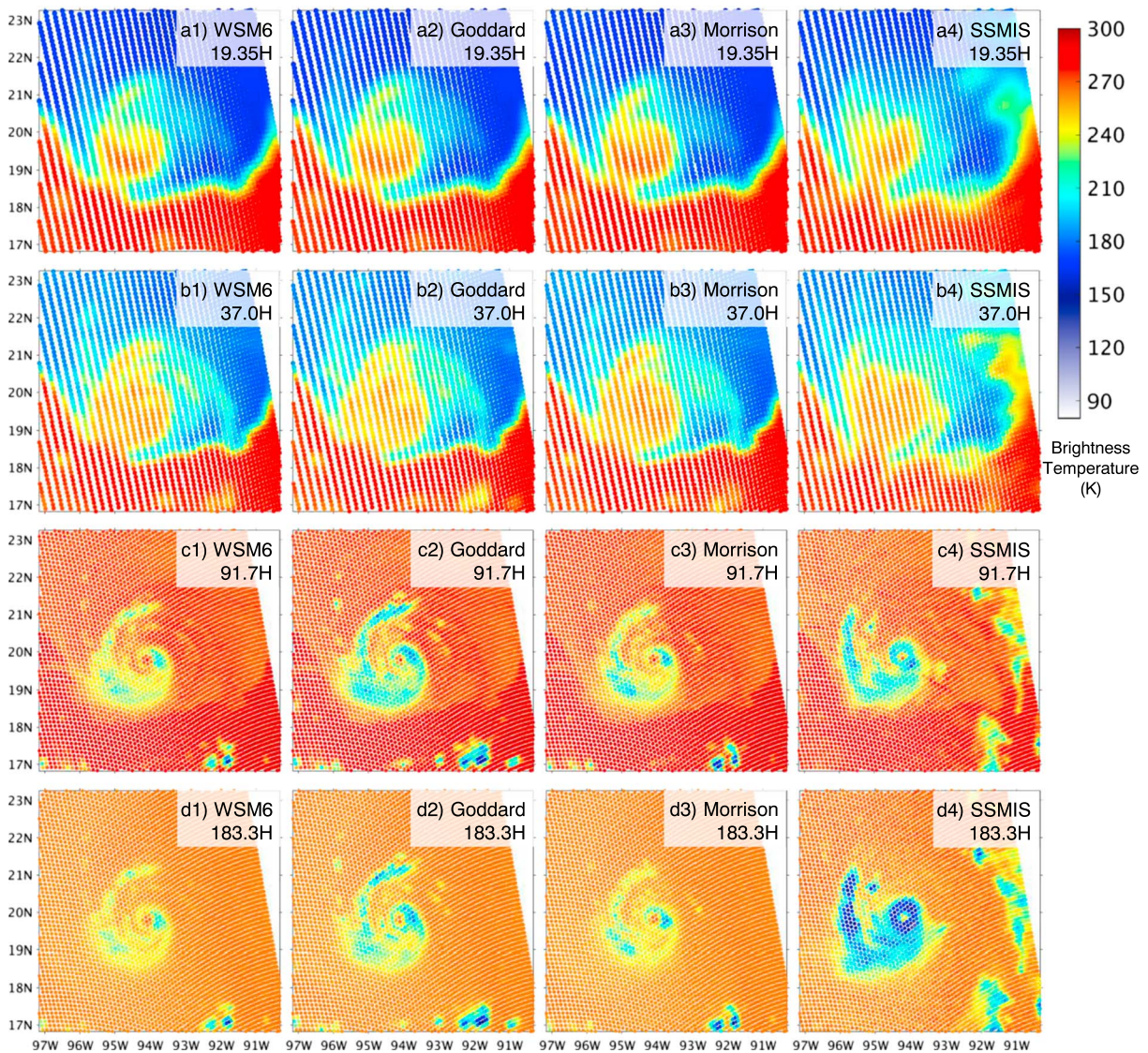
Figure 4. Same as Figure 3 but using CRTM as-released. Values of effective radius for all species but liquid and ice cloud are the ratio of third and second moments of the particle size distribution specified for each species by the respective microphysics scheme (CRTM-RE).

A sample of vertical profiles of mass mixing ratio and effective radius for each species from the WSM6 simulation is provided in Figure 2. The effective radius of a species with an exponential particle size distribution is a factor of 3 larger than the mean particle size, which is the inverse of the slope parameter, $\lambda [m^{-1}] = \left(\frac{\pi \rho N_0}{\rho_a q} \right)^{1/4}$.

For monodisperse clouds, effective radius is equal to the particle radius. Note again that CRTM-RE fixes the effective radius of all liquid and ice clouds to just 5 μm; the varying effective radii of the monodisperse liquid and ice clouds in WSM6 shown in Figure 2 are expressed only by CRTM-DS.

CRTM-RE simulated brightness temperatures are, on average, higher at all frequencies and for all microphysics schemes than those obtained with CRTM-DS: 1.9 K at 19.35H (19.35 GHz at horizontal polarization), 9.1 K at 37H, 19.4 K at 91.655H, and 19.0 K at 183.31 ± 6.6H. Figure 5 (top and middle) demonstrates that single-scattering properties in CRTM-RE are substantially different to those we calculated to be consistent with the microphysics schemes and with the same effective radius. It may seem counterintuitive that the CRTM-RE look-up table (LUT) should have greater values of scattering coefficients than the CRTM-DS LUTs, yet produce higher brightness temperatures, at a high frequency (91.665H) for which the radiance produced

Table 2. (Top) Average Error of CRTM Simulated Brightness Temperatures (in Kelvin) for the Respective Microphysics Scheme Relative to the CRTM-DS Simulated Brightness Temperatures and (Bottom) CRTM-RE and CRTM-DS Simulated Brightness Temperature Errors Relative to Observations by SSMIS Aboard Satellite DMSP-16

Frequency (GHz) and Polarization		19.35 H	37 H	91.655 H	183.31 ± 6.6 H
WSM6	RE	0.5	7.1	17.6	15.9
	DS-5μmCi	0.0	0.0	0.1	0.5
	DS-400Gp	0.2	0.8	2.5	2.0
Goddard	RE	3.7	13.7	26.4	28.1
	DS-5μmCi	2.5	3.7	6.1	12.1
Morrison	RE	1.6	6.5	14.2	13.2
	DS-5μmCi	0.0	0.0	0.1	1.6
WSM6	RE	−2.4	0.1	4.6	18.2
	DS	−2.8	−7.2	−13.0	2.3
Goddard	RE	0.3	0.3	−2.0	12.8
	DS	−3.5	−13.4	−28.4	−15.2
Morrison	RE	0.2	−0.8	3.8	17.0
	DS	−1.4	−7.3	−10.4	3.8

by precipitation is reduced by ice particle scattering at higher altitudes. However, the CRTM-RE LUT has greater values of asymmetry parameter, so not as much upwelling radiation gets scattered away from the path of the sensor or back down toward Earth. To this point, Figure 5 (bottom) compares CRTM-RE and CRTM-DS scattering phase functions for snow with the same effective radius. CRTM-RE scattering phase function represents significantly more forward scattering. The CRTM-RE LUT also has several times lower absorption coefficients.

We reran CRTM-RE and CRTM-DS at 91.655H for all three schemes but limiting cloud and precipitation input to only the liquid species—liquid cloud and rain—and one type of frozen hydrometeor—ice cloud, snow, or graupel; the differences relative to the brightness temperatures resulting from having only liquid cloud and rain for each simulation are shown in Figure 6. This experiment indicates the role of each ice species in augmenting (reducing) brightness temperatures at a high frequency. The CRTM-RE ice cloud experiment has nearly equivalent results to using just liquid species because the small water contents of ice clouds and imposed 5 μm effective radius result in the clouds being nearly transparent. For the CRTM-DS ice cloud experiments, only the Goddard scheme, which produced the largest ice cloud particles among the three schemes, has appreciable brightness temperature depressions at 91.655H. The CRTM-RE simulations have brightness temperature depressions from snow and graupel, but for all microphysics schemes the brightness temperatures that resulted from CRTM-DS are lower than those from CRTM-RE. For any combination of CRTM method and hydrometeor species, the Goddard scheme produced the lowest brightness temperatures among the three schemes. The storm area average brightness temperatures were lower with graupel than snow for the WSM6 and Goddard scheme simulation results, but lower with snow than graupel for Morrison scheme simulation results (even though graupel in Morrison, like with other schemes, produced colder localized spots). Likewise, CRTM-RE and CRTM-DS simulations are the most different from each other when graupel is simulated for WSM6 and Goddard, but differ the most with snow for Morrison.

4.2. Modified CRTM-DS Experiments

Additionally, the CRTM-DS system was used to test the significance on simulated brightness temperatures of some assumptions in the CRTM-RE single-scattering property LUT that are known to be inconsistent with one or more microphysics schemes. For these experiments, we constructed modified CRTM-DS LUTs with a specific inconsistency to the microphysics scheme.

4.2.1. Graupel Bulk Density

The bulk density of graupel is 400 kg m^{-3} in CRTM-RE, which is consistent with graupel in the Goddard and Morrison schemes, but in WSM6 graupel is 500 kg m^{-3}. Particles of different bulk densities but same mass or size have different scattering properties. Also, bulk density is a component in the slope parameter of the exponential particle size distribution for graupel in WSM6.

To test this single inconsistency within CRTM-RE in isolation of other inconsistencies, we modified the CRTM-DS LUT for WSM6 so that the bulk density of graupel was set to 400 kg m^{-3}. This change results in a given
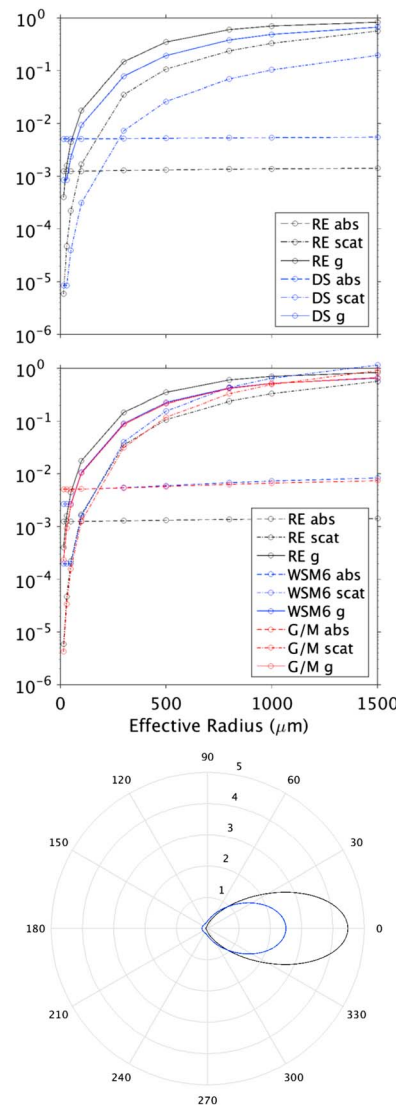
Figure 5. Comparing species properties between as-released and distribution-specific look-up tables. Asymmetry parameter (*g*), absorption coefficient [m^2 kg^{-1}] and scattering coefficient [m^2 kg^{-1}] values from the as-released look-up table and distribution-specific look-up tables for (top) snow and (middle) graupel. All three schemes produce the same values for snow, but WSM6 has a different graupel bulk density than Goddard and Morrison (G/M). Scattering phase function of 1000 μm (bottom) effective radius snow from the as-released look-up table (black) and distribution-specific look-up tables (blue).

water content of graupel to be composed of a greater number of particles with a greater mass-weighted average size.

Figure 7 shows the brightness temperatures from using the correct and modified WSM6 CRTM-DS LUT, and Table 2 (upper half) contains summary statistics. The experiment with the less dense graupel (400 kg m^{-3}) produced higher brightness temperatures; for example, most of the cloud shield is at least 6 K warmer at 91.655H.

4.2.2. Ice Cloud Particle Size

In CRTM-RE, all liquid and ice clouds are assigned an effective radius of 5 μm, and ice clouds have a bulk density of 900 kg m^{-3} (equivalent to that of hail). In contrast, the ice cloud particles produced by all three microphysics schemes are of different bulk density, and some are large enough to have the capability of scattering significant amounts of microwave radiation: effective radii are as high as 250 μm in WSM6 (monodisperse; hard limit), 1050 μm in Morrison (double-moment exponential; hard limit), and greater than 3000 μm in Goddard (monodisperse).

We constructed modified CRTM-DS LUTs for each microphysics scheme, labeled CRTM-DS-5μmCi, in which the consistent ice cloud scattering properties are replaced with those for monodisperse ice spheres of 5 μm radius having a bulk density of 900 kg m^{-3}, and compared the resulting brightness temperatures with those from CRTM-DS simulations. (For s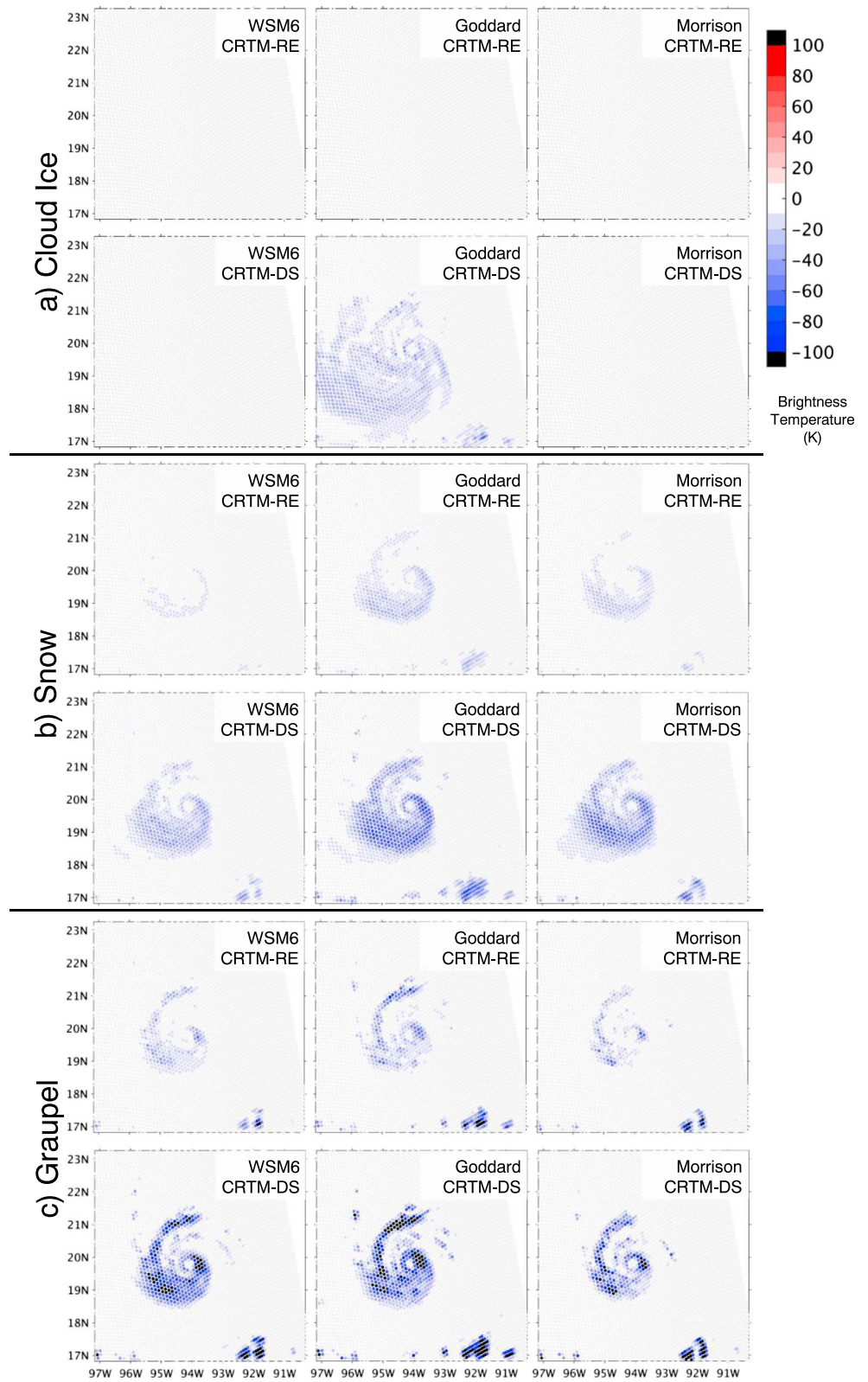uch a low value of effective radius, the choice of particle size distribution is inconsequential to the resulting brightness temperature.) Note that there are discrepancies in liquid cloud particle sizes between CRTM-RE and the microphysics schemes, but they are much smaller than the ice cloud discrepancies so were not investigated.

Figure 8 shows the differences in simulated brightness temperatures between the CRTM-DS-5μmCi and CRTM-DS experiments, and Table 2 (upper half) contains summary statistics. As expected, the scheme producing the largest ice cloud particles, the Goddard scheme, had the greatest differences in brightness temperature from CRTM-DS. The extensive area of ice cloud scattering to the south and west of the hurricane at all frequencies (though not readily apparent at 19.35H) diminished resulting in significant increases in brightness temperature relative to CRTM-DS. Furthermore, in the area of highest 19.35H brightness temperatures near the core of the hurricane brightness temperatures also increased. The Morrison scheme also warmed

Figure 6. Difference in 91.665 GHz brightness temperatures between using only cloud liquid and rain, and the further addition of either (a) ice cloud, (b) snow, or (c) graupel hydrometeor species.
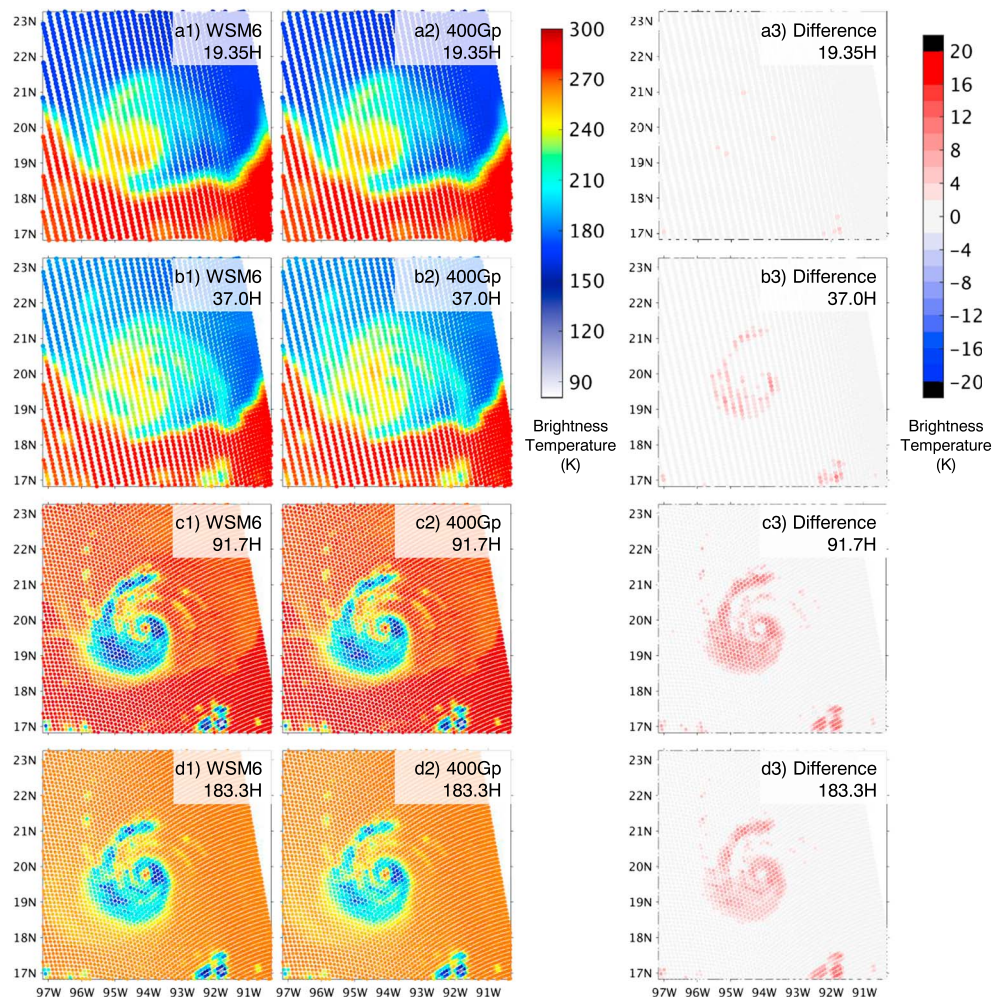
Figure 7. WSM6 CRTM-DS using (a1, b1, c1, and d1) the scheme-consistent 500 kg m^{-3} bulk density of graupel and (center) 400 kg m^{-3} bulk density of graupel; (a2, b2, c2, and d2) 400 kg m^{-3} minus 500 kg m^{-3} CRTM-DS brightness temperatures.

slightly at 183.31 ± 6.6H, as did WSM6 (though by less than 5 K at all locations). For CRTM-DS-5µmCi, the Goddard scheme remained the coldest of the three schemes, despite having warmed the most relative to CRTM-DS.

The average of the root-mean-square differences of the brightness temperatures between schemes across all frequencies when using CRTM-DS-5µmCi is 13.7 K, which is substantially less than the 16.2 K obtained for CRTM-DS. That is, making the ice cloud scattering properties uniform between schemes (and much closer to the extreme values in CRTM-RE) reduced the brightness temperature differences between the microphysics scheme results. However, these differences are still substantially greater than the differences between the schemes when applying CRTM-RE to their outputs (9.4 K).

5. Concluding Remarks

In what follows we first summarize the differences between CRTM-RE and CRTM-DS and the shortcomings of using scattering property LUTs based only on effective radius. Our findings, like those for many earlier studies, indicate potential problems in using spheres to represent the scattering properties of nonspherical ice particles; in the last sections of what follows we attempt to put our results into the proper context of these earlier studies.
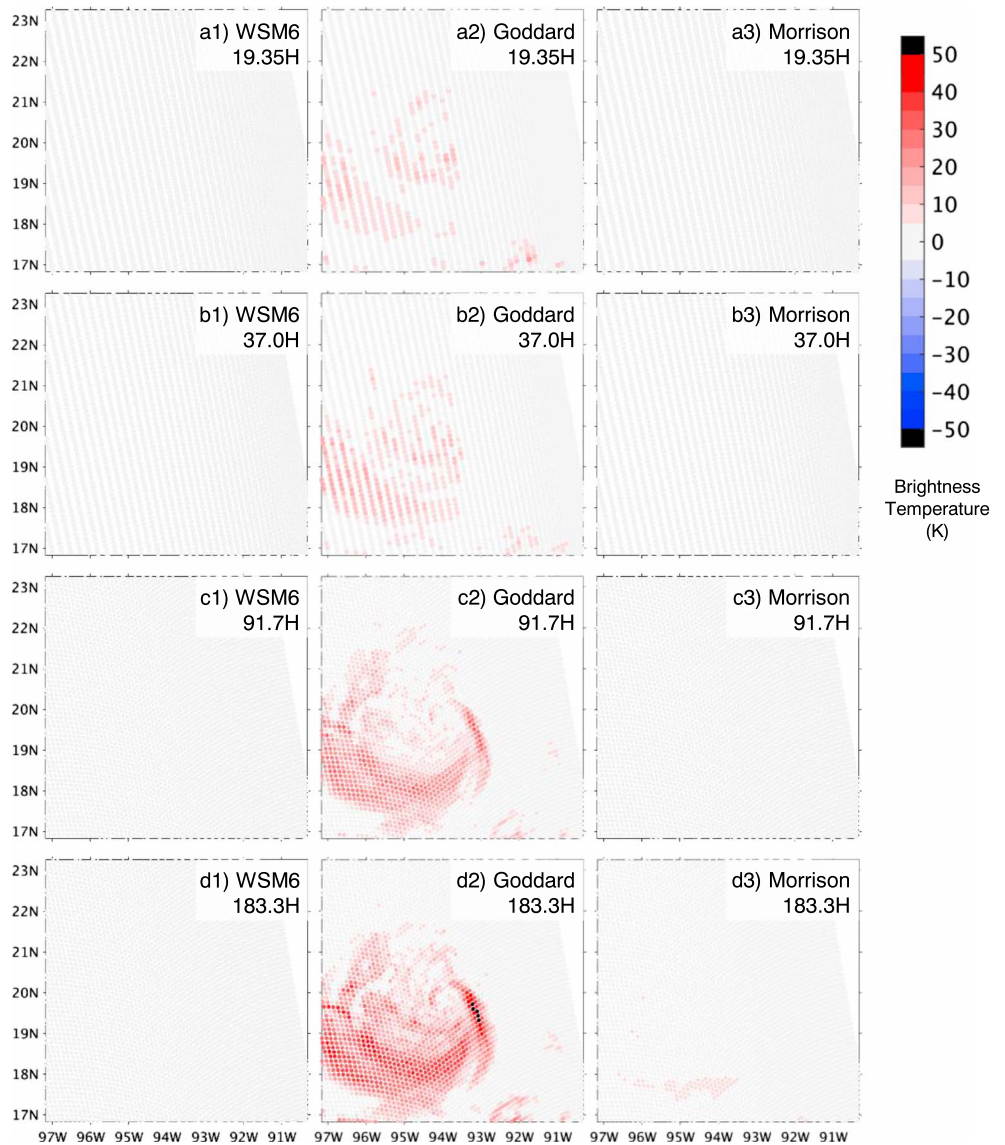
Figure 8. Difference in brightness temperatures between the modified CRTM-DS in which the scheme-consistent ice cloud scattering properties are replaced by those for a 5 mm monodisperse ice cloud (CRTM-DS-5μmCi) and CRTM-DS.

5.1. Summary of Findings

The CRTM was modified to use cloud and precipitation single-scattering properties that are consistent with the particle properties and size distributions as specified inside the WSM6, Goddard, and Morrison microphysics parameterization schemes in the WRF model. The "Distribution-Specific" CRTM (CRTM-DS) retains from the CRTM as-released the concept of using single-scattering look-up tables (LUTs) for each hydrometeor species but is different in that a uniquely consistent scattering LUT is constructed for each microphysics scheme. A large set of Mie computations for spherical liquid and ice particles with varying size, bulk density (ice), and temperature (liquid) at many frequencies across the microwave spectrum provided the data for these LUTs.

With 3 h, 3 km grid spacing WRF forecasts for Hurricane Karl (2010) using different microphysics schemes as a test case, we computed brightness temperatures with CRTM-DS and with the CRTM as-released using scheme-consistent cloud effective radii as inputs to it, which we refer to as CRTM-RE. For Goddard, WSM6, and Morrison microphysics schemes, and at all frequencies, the CRTM-RE brightness temperatures were substantially warmer than CRTM-DS brightness temperatures. The Goddard scheme

simulation produced the lowest brightness temperatures in every experiment. Depending on the microphysics scheme, either snow or graupel is primarily responsible for brightness temperature depressions across the hurricane at 91.655 GHz.

So little about the CRTM-RE LUT construction is known that the ultimate sources of the bias and inconsistent cloud single-scattering properties cannot be determined. Even if our assumption that the CRTM-RE LUT was generated from Mie computations is correct, possible inconsistencies with our methodology include the method for mixing ice and air within a soft sphere, the dielectric constants of ice and water, the limits and resolution of the numerical integration over the particle size distribution, and the source of scattering phase functions. The (implied) absorption coefficients of snow and graupel for all effective radii in the CRTM-RE look-up table are lower than those for all particle sizes of corresponding bulk density in our database; therefore, we know that ice particle absorption properties are inconsistent. However, the decisions made in developing CRTM-DS LUTs were foremost motivated to be consistent with CRTM-RE when known and possible (e.g., temperature-dependent liquid dielectric constants and no temperature-dependent ice dielectric constants); otherwise, the development decisions made were believed to produce equivalent or superior results to what is in the CRTM-RE LUTs for the purpose of microphysics consistency (e.g., modern values of ice and water dielectric constants, using an integration upper limit diameter as high as 20000 μm, and using scattering phase functions direct from Mie computations instead of a parameterization). Of course, inconsistent particle size distributions are a possible source for discrepant single-scattering properties, for which CRTM-DS is designed to address specifically.

Two specific inconsistencies between CRTM-RE and microphysics schemes—ice cloud particle sizes and graupel bulk density—were investigated. A change in bulk density of graupel from 400 kg m^{-3} to 500 kg m^{-3} in the representation of graupel (exponential particle size distribution) single-scattering properties caused differences in brightness temperatures of several Kelvin across much of the hurricane at some frequencies. *Doherty et al.* [2007] also found sensitivity of brightness temperature to ice bulk density. The 5 μm effective radius assumed for ice clouds in CRTM-RE was much less than the output of all microphysics schemes, but replacing microphysics-consistent particle sizes and bulk densities resulted in meaningfully higher brightness temperatures only for Goddard simulation at all tested frequencies and the highest frequency for the Morrison simulation.

5.2. Comparing to Observations

CRTM-DS produced some unrealistically low brightness temperature fields, as evidenced by the SSMIS observations of Hurricane Karl shown in this study (Figure 3). All simulations at 37H (37 GHz horizontal polarization) and 91.665H were cold-biased. In contrast, 183.31H generally had a warm bias. Future research will examine if this is a systematic bias through direct comparisons of CRTM-DS simulated brightness temperatures with satellite observations for multiple events under different environmental conditions. The low-biased brightness temperatures at imaging frequencies close to 91.665H in CRTM-DS have been observed with other microphysics-consistent hydrometeor scattering radiative transfer computed from WRF output [e.g., *Han et al.*, 2013; *Masunaga et al.*, 2010] and other cloud-resolving models [e.g., *Li et al.*, 2010; *Matsui et al.*, 2016]. Scheme-consistent single-scattering properties is not a deliberate mechanism for impacting (reducing or amplifying) simulation-observation bias, rather its primary motivation is to produce more meaningful correlations between brightness temperatures and modeled atmospheric states. Accurate and consistent single-scattering properties in radiative transfer would be crucial for attempting to validate or constrain microphysics schemes with microwave (passive or active radar) observations [e.g., *Wiedner et al.*, 2004; *Meirold-Mautner et al.*, 2007; *Matsui et al.*, 2009, 2014, 2016; *Han et al.*, 2013; *Hashino et al.*, 2013; *Li et al.*, 2010].

Significant biases between observed and simulated brightness temperatures in scenes containing precipitation would be difficult to overcome in data assimilation procedures. If using CRTM-DS as the observation operator, then perhaps the greatest challenge would be at 37.0H (see Figure 3b): in some areas of active deep convection the simulated brightness temperatures are nearly as low as clear sky over the ocean, and the highest brightness temperatures are at locations with some rain and only light to moderate mixing ratios of snow and graupel. This is not a quasi-linear and one-to-one relationship between precipitation intensity and brightness temperature that would seem necessary for developing physically meaningful statistical relationships for application in modern data assimilation techniques.

The many potential sources of inconsistencies contributing to the differences and biases in brightness temperatures between CRTM-DS and observations include unrealistic microphysics scheme mixing ratios, particle properties, and particle size distributions. For example, the Goddard scheme produces very massive (precipitation-sized) ice cloud particles, which impacts brightness temperatures at all frequencies in a manner not consistent with observations. However, it may be suitable in at least certain applications of microphysics-consistent radiative transfer to simply disregard such grossly inaccurate particle properties, instead of working to remove their existence in the scheme and subsequent model output, if the latter jeopardizes the evolution of seemingly reasonable water contents of precipitation species.

The temperature of ice particles is another source of inconsistency. Temperature changes both the imaginary and real parts of the dielectric constant. The CRTM as-released does not currently support a temperature dimension in the scattering look-up tables for ice species. Likewise, CRTM-DS supports a temperature dimension only for species with temperature-dependence in the particle size distribution, namely, WSM6 snow and Goddard cloud ice. We tested the sensitivity to ice temperature by assuming a constant and very low ice temperature of 163.15 K. For this one case the absorption coefficients dropped significantly, but brightness temperatures were relatively unchanged (not shown).

5.3. Spherical Versus Nonspherical Particle Scattering Properties

Much research has been conducted at microwave wavelengths on the overall suitability of approximating the complex shapes of real ice particles as spheres and applying Mie theory [e.g., *Hong*, 2007; *Liu*, 2008; *Baran et al.*, 2011; *Geer and Baordo*, 2014]. The differences in the single-scattering properties between spherical and real ice particles may be another major factor responsible for (climatological) biases between simulated brightness temperatures from model output and observed brightness temperatures. One concern with applying Mie theory to scattering for particle sizes larger than the wavelength is unrealistic treatment of resonances and the presence of features, e.g., halo peaks, in the scattering phase functions. We observed these halo peaks in our exact Mie scattering phase function computations for individual particles, but they smoothed out when integrating over an exponential particle size distribution. However, integration does not remove persistent biases in forward versus backward scattering and this likely leads to biases between modeled and observed brightness temperatures when using spheres to represent the scattering properties of real, nonspherical particles [e.g., *Olson et al.*, 2016; *Kuo et al.*, 2016].

Though CRTM-RE produced substantially higher brightness temperatures than CRTM-DS, it also produced some unrealistic brightness temperature fields. All simulations at 183.31H were severely warm biased, and 91.665H is generally somewhat warm-biased. This apparent inconsistency in scattering between ~37 GHz and ~183 GHz has been identified as a consequence of using spherical particle scattering, regardless of bulk density and particle size distribution [*Surussavadee and Staelin*, 2006; *Geer and Baordo*, 2014]; our CRTM-RE and CRTM-DS simulations offer further evidence toward this assertion.

The use of complex particle geometries instead of spheres for the single-scattering properties of ice species would likely better represent the scattering of natural hydrometeors, and certain particle shapes may reduce biases of CRTM-DS simulated brightness temperatures relative to observations. This approach is on the forefront of atmospheric radiative transfer research within operational data assimilation [e.g., *Geer and Baordo*, 2014; *Eriksson et al.*, 2015]. However, *Surussavadee and Staelin* [2006] and *Liu* [2004] have demonstrated that frequency-dependent adjustments to ice particle densities within the context of spherical particle scattering can be used to remove observation to model brightness temperature biases. And *Honeyager et al.* [2016] showed that more realistic estimates of ice particle density within the context of spheroidal particle scattering may also hold promise.

It is common among microphysics schemes, including the three tested here (except for ice cloud in WSM6), that the distribution of mass among individual particles is described assuming that all hydrometeors are spheres; however, some schemes, like Thompson [*Thompson et al.*, 2008] and Milbrandt-Yau [*Milbrandt and Yau*, 2005; *Milbrandt et al.*, 2009], deviate from this simple assumption for snow. To use particles having a mass-size relationship that differs from that specified by a microphysics scheme (whether spherical or not) would naturally cause inconsistency with the scheme-specified number concentration, particle sizes, and/or particle masses. The implications of such a substitution within the philosophy of microphysics-consistent radiative transfer is worthy of consideration.
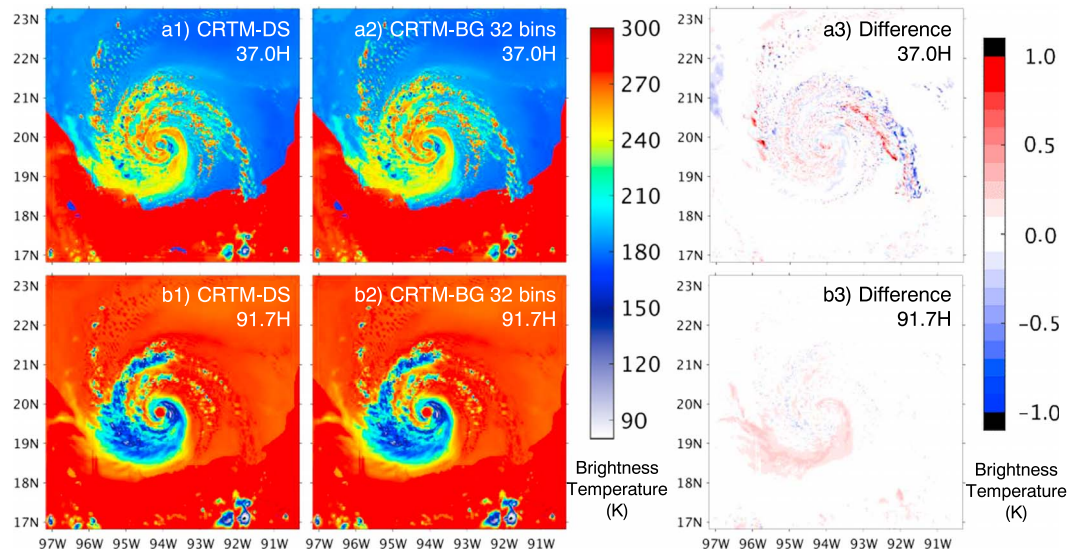
Figure 9. (2) CRTM-BG brightness temperatures from the WSM6 simulation using 32 bins to discretize the particle size distribution, and (1) CRTM-DS results. (3) CRTM-BG minus CRTM-DS brightness temperatures.

As discussed in section 2, the use of spherical particle scattering in this study is appropriate, where the CRTM-DS is used to explore sensitivities in radiative transfer to different representations of cloud microphysics. Using spheres offers trivial and exact consistency with both the particle size and mass distributions. It also matches the presumed construction method of the CRTM as-released LUT, thus eliminating particle shape as a potential source of bias between CRTM-RE and CRTM-DS simulations.

5.4. Valued Modifications to CRTM

Slant path construction, precise antenna pattern convolution, and ice temperature would be necessary additions to the CRTM in order to rigorously compare simulated and observed brightness temperatures in areas of precipitation, especially deep moist convection. For example, in the present simulations, near vertical columns of high graupel mass associated with active convective cells led to exceptionally low brightness temperatures at low-mid frequencies (e.g., 37.0 GHz). As demonstrated in the approximate form implemented here, antenna pattern convolution works to diffuse smaller areas of very low brightness temperature within the generally warm hurricane cloud field. In addition, a slant path construction would spread the high amounts of graupel found in near vertical columns of deep moist convection across many slant paths, so no single slant path would have as much scattering and as low a brightness temperature as a vertical path centered on a cell of convection. Finally, the temperature of ice changes its absorption and scattering properties, so this effect should be represented.

Slant path construction, satellite antenna gain patterns, and microphysics consistency are among the features found in delta-Eddington two-stream satellite simulators such as Goddard Satellite Data Simulator Unit [*Matsui et al.*, 2014; *Masunaga et al.*, 2010]. However, satellite simulators are exclusively forward models; tangent-linear and adjoint models are important to users of the CRTM in variational data assimilation systems. We attempted to make corresponding modifications to the existing CRTM tangent-linear and adjoint codes for CRTM-DS, but they have not been tested. It may be necessary to apply expertise with the tangent linear and adjoint of specific microphysics schemes to produce satisfactory results.

It is also entirely possible to achieve microphysics consistency by constructing scattering LUTs which interface by effective radius, but designed with and designated for specific particle properties and size distributions. For example, all three schemes studied here may share a single effective radius LUT for snow (see Figure 5, top); the consequence of their differences in determining number concentration (see Appendix A) is that snow of a given water content will differ in effective radius. This method could ease development of tangent linear and adjoint models; the existing models may already be suitable. However, CRTM-DS does not burden the user with calculating scheme-consistent effective radii in order to achieve -microphysics-consistency.

We developed a second method for building microphysics-scheme-consistent radiative properties called Bin-Generalized (CRTM-BG) (Figure 9). Instead of using scattering property LUTs of integrated particle size distributions, this method utilizes scattering property LUTs of individual liquid and ice particles, and integration over particle mass distributions is performed within the CRTM. The two primary merits of the Bin-Generalized method are being a more intuitive method for supporting bin microphysics schemes, like the one-moment HUJI spectral bin model in WRF [*Khain et al.*, 2004], and for any experiments in which bulk densities or certain parameter values of particle size distributions (such as making a nonzero shape parameter of a generalized gamma distribution) are not fixed spatially or temporally. As it now stands, CRTM-BG has only a forward model.

All of the modified versions of the CRTM discussed will be made available to the public for use. We intend to work with the CRTM development community toward advancing future released versions of CRTM that go beyond use of a single-scattering property look-up table interfaced with effective radius.

Appendix A: Microphysics Parameterization Scheme Details

The three microphysics schemes used in this study are WRF Single-Moment 6-Class (WSM6) [*Dudhia et al.*, 2008], Goddard (single-moment [*Lang et al.*, 2007]), and Morrison (double-moment [*Morrison et al.*, 2009]) as they are in the WRF model version 3.6.1. Provided here is information on how each scheme, hence its associated CRTM-DS look-up table, specifies the species, as well as all what little is known (e.g., particle densities) or safely presumed about the CRTM-RE look-up table.

The double-moment species in Morrison have mixing ratio and number concentration predicted.

A1. Cloud Liquid

Cloud liquid has a monodisperse distribution in WSM6 and Goddard. WSM6 has a fixed number concentration $N_c[\text{m}^{-3}] = 3.0 \times 10^6$; therefore, the particle size responds to changes in water content. In contrast, Goddard has a fixed particle diameter of 20 μm; therefore, the number concentration varies between clouds.

In Morrison, cloud liquid has a gamma distribution. In these simulations, the scheme is configured to predict only a single moment: the number concentration is fixed ($N_c[\text{m}^{-3}] = 2.5 \times 10^6$), and therefore the shape parameter is fixed as well ($\mu_c = 4.827$). The gamma distribution is formulated as

$$N_c(D_c) = N_{0,c} D_c{}^{\mu_c} e^{-\lambda_c D_c},$$

where the slope parameter $\lambda_c[\text{m}^{-1}] = \left[\frac{\pi \rho_c N_c \Gamma(\mu_c+4)}{6 q_c \Gamma(\mu_c+1)} \right]^{\frac{1}{3}}$, where $\frac{(\mu_c+1)}{60.0 \times 10^{-6}} \leq \lambda_c \leq \frac{(\mu_c+1)}{1.0 \times 10^{-6}}$ (or roughly $9.71 \times 10^4 \leq \lambda_c \leq 5.83 \times 10^6$ for $\mu_c = 4.827$), and the intercept parameter $N_{0,c} \left[\text{kg}^{-1} \text{m}^{-1} \right] = \frac{N_c \lambda_c{}^{\mu_c+1}}{\Gamma(\mu_c+1)}$.

For the CRTM look-up table as currently released, all liquid clouds are given the scattering properties of a rain cloud having an effective radius of 5 μm. Specifications of the liquid cloud particle size distribution are unknown.

All assume nearly the same liquid particle density: 1000 kg m^{-3} in WSM6 and Goddard, and 997 kg m^{-3} in Morrison.

A2. Cloud Ice

Cloud ice has a monodisperse distribution in WSM6. A set of equations relates cloud ice content ($\rho_a q_i$) to number concentration, particle radius, and particle density:

1. Number concentration: $N_i[\text{m}^{-3}] = 5.38 \times 10^7 (\rho_a q_i)^{0.75}$, where $10^3 \leq N_i \leq 10^6$
2. Particle mass: $M_i[\text{kg}] = (\rho_a q_i)/N_i$
3. Particle radius: $R_i[\text{m}] = 5.95 M_i{}^{1/2}$, where $R_i \leq 250.0 \times 10^{-6}$
4. Density of equivalent sphere: $\rho_i[\text{kg} \cdot \text{m}^{-3}] = \frac{M_i}{(\pi/6) D_i{}^3}$

As determined by the equations and the bounds on parameter values, the density of the equivalent sphere can range from that of solid ice (917 kg m^{-3}) to less than 100 kg m^{-3}.

Cloud ice also has a monodisperse distribution in Goddard. The cloud ice particle concentration is specified by the *Fletcher* [1962] equation:

$$N_i \left[m^{-3} \right] = n_0 e^{\beta \Delta T},$$

with $\Delta T[K] = 273.15 - T$. The Goddard scheme uses the values $n_0 = 10^{-6}$ and $\beta = 0.46$. Particle density is that of solid ice (917 kg m^{-3}).

Cloud ice has an exponential distribution in Morrison and is two-moment (mixing ratio and number concentration). The slope parameter value is bounded by $\frac{1}{(2 \times 125.0 \times 10^{-6}) + 100.0 \times 10^{-6}} \leq \lambda_i \leq \frac{1}{10^{-6}}$ (or roughly $2.86 \times 10^3 \leq \lambda_i \leq 10^6$). Particle density is 500 kg m^{-3}.

For the CRTM look-up table as currently released, all ice clouds are given the scattering properties of a hail cloud having an effective radius of 5 μm. Particle density is 900 kg m^{-3}, but other specifications of the particle size distribution are unknown. This small particle size makes ice clouds of realistic water contents to be virtually invisible in simulations at microwave wavelengths.

A3. Rain

Rain has an exponential distribution in all schemes and is double-moment in Morrison. WSM6 and Goddard follow a *Marshall and Palmer* [1948] distribution with $N_r[m^{-3}] = 8.0 \times 10^6$, although WSM6 limits the slope parameter $\lambda_r[m^{-1}] \leq 8.0 \times 10^4$. Morrison bounds the slope parameter by $\frac{1}{2800.0 \times 10^{-6}} \leq \lambda_r \leq \frac{1}{20.0 \times 10^{-6}}$ (or roughly $3.57 \times 10^2 \leq \lambda_r \leq 5.00 \times 10^4$).

All assumes nearly the same particle density (same as cloud liquid).

A4. Snow

Snow has an exponential distribution in all schemes and is double-moment in Morrison. For WSM6, the snow particle number concentration is a function of temperature (Kelvin):

$$N_{0,s} \left[m^{-3} \cdot m^{-1} \right] = 2.0 \times 10^6 e^{0.12(273.15-)T},$$

limited $N_{0,s} \leq 10^{11}$ (a value produced at 183 K), and the slope parameter is limited $\lambda_s[m^{-1}] \leq 10^5$. Goddard assumes a fixed number concentration $N_s[m^{-3}] = 1.6 \times 10^7$. Morrison bounds the slope parameter by $\frac{1}{2000.0 \times 10^{-6}} \leq \lambda_s \leq \frac{1}{10.0 \times 10^{-6}}$ (or $5.0 \times 10^2 \leq \lambda_s \leq 10^5$).

All assumes the same particle density of 100 kg m^{-3}.

A5. Graupel

Graupel has an exponential distribution in all schemes and is double-moment in Morrison. WSM6 and Goddard assume a number concentration $N_g[m^{-3}] = 4.0 \times 10^6$. WSM6 limits the slope parameter $\lambda_g[m^{-1}] \leq 6.0 \times 10^4$. Morrison bounds the slope parameter by $\frac{1}{2000.0 \times 10^{-6}} \leq \lambda_g \leq \frac{1}{20.0 \times 10^{-6}}$ (or $5.0 \times 10^2 \leq \lambda_g \leq 5.0 \times 10^5$).

The WSM6 scheme assumes a different particle density (500 kg m^{-3}) than Goddard, Morrison, and the CRTM-RE look-up Table (400 kg m^{-3}). The simulation with the Morrison scheme is configured to model graupel as heavy ice precipitation (hail is the other option).

References

Baran, A., A. Bodas-Salcedo, R. Cotton, and C. Lee (2011), Simulating the equivalent radar reflectivity of cirrus at 94 GHz using an ensemble of cirrus ice crystals: A test of the Met Office global numerical weather prediction model, *Q. J. R. Meteorol. Soc.*, *137*, 1547–1560, doi:10.1002/qj.870.

Baran, A., P. Hill, K. Furtado, P. Field, and J. Manners (2014), A coupled cloud physics–radiation parameterization of the bulk optical properties of cirrus and its impact on the Met Office Unified Model Global Atmosphere 5.0 configuration, *J. Clim.*, *27*, 7725–7752, doi:10.1175/JCLI-D-13-00700.1.

Baran, A., P. Hill, D. Walters, S. C. Hardiman, K. Furtado, P. R. Field, and J. Manners (2016), The impact of two coupled cirrus microphysics-radiation parameterizations on the temperature and specific humidity biases in the tropical tropopause layer in a climate model, *J. Clim.*, *29*, 5299–5316, doi:10.1175/JCLI-D-15-0821.1.

Bao, Y., J. Xu, A. M. Powell Jr., M. Shao, J. Min, and Y. Pan (2015), Impacts of AMSU-A, MHS and IASI data assimilation on temperature and humidity forecasts with GSI–WRF over the western United States, *Atmos. Meas. Tech.*, *8*, 4231–4242, doi:10.5194/amt-8-4231-2015.

Bennartz, R. (2000), Optimal convolution of AMSU-B to AMSU-A, *J. Atmos. Oceanic Technol.*, *17*, 1215–1225.

Bohren, C. F., and D. R. Huffman (1983), *Absorption and Scattering of Light by Small Particles*, pp. 477–482, John Wiley, New York.

Doherty, A. M., T. R. Sreerekha, U. M. O'Keeffe, and S. J. English (2007), Ice hydrometeor microphysical assumptions in radiative transfer models at AMSU-B frequencies, *Q. J. R. Meteorol. Soc.*, *133*, 1205–1212.

Dudhia, J., S. Y. Hong, and K. S. Lim (2008), A new method for representing mixed-phase particle fall speeds in bulk microphysics parameterizations, *J. Meteorol. Soc. Jpn.*, *86A*, 33–44, doi:10.2151/jmsj.86A.33.

Eriksson, P., M. Jamali, J. Mendrok, and S. A. Buehler (2015), On the microwave optical properties of randomly oriented ice hydrometeors, *Atmos. Meas. Tech.*, *8*, 1913–1933, doi:10.5194/amt-8-1913-2015.

Fletcher, N. H. (1962), *The Physics of Rainclouds*, 386 pp., Cambridge Univ. Press, U. K., and New York.

Geer, A. J., and F. Baordo (2014), Improved scattering radiative transfer for frozen hydrometeors at microwave frequencies, *Atmos. Meas. Tech.*, *7*, 1839–1860, doi:10.5194/amt-7-1839-2014.

Geer, A. J., and P. Bauer (2011), Observation errors in all-sky data assimilation, *Q. J. R. Meteorol. Soc.*, *137*, 2024–2037, doi:10.1002/qj.830.

Greenwald, T., R. Bennartz, C. O'Dell, and A. Heidinger (2004), Fast computation of microwave radiances for data assimilation using the successive order of scattering approximation, *J. Appl. Meteorol.*, *44*, 960–966, doi:10.1175/JAM2239.1.

Han, M., S. A. Braun, T. Matsui, and C. R. Williams (2013), Evaluation of cloud microphysics schemes in simulations of a winter storm using radar and radiometer measurements, *J. Geophys. Res. Atmos.*, *118*, 1401–1419, doi:10.1002/jgrd.50115.

Han, Y., P. van Delst, Q. Liu, F. Weng, B. Yan, R. Treadon, and J. Derber (2006), JCSDA Community Radiative Transfer Model (CRTM)—Version 1, NOAA Tech. Report 122.

Hansen, J. E., and I. D. Travis (1974), Light scattering in planetary atmospheres, *Space Sci. Rev.*, *16*, 527–610.

Hashino, T., M. Satoh, Y. Hagihara, T. Kubota, T. Matsui, T. Nasuno, and H. Okamoto (2013), Evaluating cloud microphysics from NICAM against CloudSat and CALIPSO, *J. Geophys. Res. Atmos.*, *118*, 1–20, doi:10.1002/jgrd.50564.

Honeyager, R., G. Liu, and H. Nowell (2016), Voronoi diagram-based spheroid model for microwave scattering of complex snow aggregates, *J. Quant. Spectrosc. Radiat. Transfer*, *170*, 28–44, doi:10.1016/j.jqsrt.2015.10.025.

Hong, G. (2007), Parameterization of scattering and absorption properties of nonspherical ice crystals at microwave frequencies, *J. Geophys. Res.*, *112*, D11208, doi:10.1029/2006JD008364.

Kazumori, M., A. J. Geer, and S. J. English (2016), Effects of all-sky assimilation of GCOM-W/AMSR2 radiances in the ECMWF numerical weather prediction system, *Q. J. R. Meteorol. Soc.*, *142*, 721–737.

Khain, A., A. Pokrovsky, M. Pinsky, A. Seifert, and V. Phillips (2004), Simulation of effects of atmospheric aerosols on deep turbulent convective clouds using a spectral microphysics mixed-phase cumulus cloud model. Part I: Model description and possible applications, *J. Atmos. Sci.*, *61*, 2963–2982, doi:10.1175/JAS-3350.1.

Kuo, K., W. Olson, B. Johnson, M. Grecu, L. Tian, T. Clune, B. van Aartsen, A. Heymsfield, L. Liao, and R. Meneghini (2016), The microwave radiative properties of falling snow derived from nonspherical ice particle models. Part I: An extensive database of simulated pristine crystals and aggregate particles, and their scattering properties, *J. Appl. Meteorol. Climatol.*, *55*, 691–708, doi:10.1175/JAMC-D-15-0130.1.

Lang, S., W.-K. Tao, R. Cifelli, W. Olson, J. Halverson, S. Rutledge, and J. Simpson (2007), Improving simulations of convective system from TRMM LBA: Easterly and westerly regimes, *J. Atmos. Sci.*, *64*, 1141–1164, doi:10.1175/JAS3879.1.

Li, X., W.-K. Tao, T. Matsui, C. Liu, and H. Masunaga (2010), Improving a spectral bin microphysical scheme using long-term TRMM satellite observations, *Q. J. R. Meteorol. Soc.*, *136*, 382–399.

Liu, G. (2004), Approximation of single scattering properties of ice and snow particles for high microwave frequencies, *J. Atmos. Sci.*, *61*, 2441–2456, doi:10.1175/1520-0469(2004)061,2441:AOSSPO.2.0.CO;2.

Liu, G. (2008), A database of microwave single-scattering properties for nonspherical ice particles, *Bull. Am. Meteorol. Soc.*, *89*, 1563–1570.

Liu, Q., and F. Weng (2006), Advanced doubling-adding method for radiative transfer in planetary atmospheres, *J. Atmos. Sci.*, *63*, 3459–3465, doi:10.1175/JAS3808.1.

Marshall, J. S., and W. M. Palmer (1948), The distribution of raindrops with size, *J. Meteor.*, *5*, 165–166, doi:10.1175/1520-0469(1948) 005<0165:TDORWS>2.0.CO;2.

Masunaga, H., et al. (2010), Satellite data simulator unit: A multisensor, multispectral satellite simulator package, *Bull. Am. Meteorol. Soc.*, *91*, 1625–1632, doi:10.1175/2010BAMS2809.1.

Matsui, T., X. Zeng, W.-K. Tao, H. Masunaga, W. Olson, and S. Lang (2009), Evaluation of long-term cloud-resolving model simulations using satellite radiance observations and multifrequency satellite simulators, *J. Atmos. Oceanic Technol.*, *26*, 1261–1274, doi:10.1175/2008JTECHA1168.1.

Matsui, T., et al. (2014), Introducing multisensor satellite radiance-based evaluation for regional Earth system modeling, *J. Geophys. Res. Atmos.*, *119*, 8450–8475, doi:10.1002/2013JD021424.

Matsui, T., J. Chern, W.-K. Tao, S. Lang, M. Satoh, T. Hashino, and T. Kubota (2016), On the land-ocean contrast of tropical convection and microphysics statistics derived from TRMM satellite signals and global storm-resolving models, *J. Hydrometeorol.*, *17*, 1425–1445, doi:10.1175/JHM-D-15-0111.1.

Melhauser, C., F. Zhang, Y. Weng, Y. Jin, H. Jin, and Q. Zhao (2017), A multiple-model convection-permitting ensemble examination of the probabilistic prediction of tropical cyclones: Hurricanes Sandy (2012) and Edouard (2014), *Weather Forecasting*, *32*, 665–688, doi:10.1175/WAF-D-16-0082.1.

Meirold-Mautner, I., C. Prigent, E. Defer, J. R. Pardo, J.-P. Chaboureau, J.-P. Pinty, M. Mech, and S. Crewell (2007), Radiative transfer simulations using mesoscale cloud model outputs: Comparisons with passive microwave and infrared satellite observations for midlatitudes, *J. Atmos. Sci.*, *64*, 1550–1568, doi:10.1175/JAS3896.1.

Milbrandt, J. A., and M. K. Yau (2005), A multimoment bulk microphysics parameterization. Part I: Analysis of the role of the spectral shape parameter, *J. Atmos. Sci.*, *62*, 3051–3064.

Milbrandt, J. A., R. McTaggart-Cowan, and D. Jacob (2009), Forecasting the solid-to-liquid ratio of precipitation in a cloud-resolving model. Preprints, *23rd Conf. on Weather, Analysis, and Forecasting/19th Conf. on Numerical Weather Prediction*, Am. Meteorol. Soc., 7A2, Omaha, Nebr. [Available at http://ams.confex.com/ams/pdfpapers/154287.pdf.]

Morrison, H., G. Thompson, and V. Tatarskii (2009), Impact of cloud microphysics on the development of trailing stratiform precipitation in a simulated squall line: Comparison of one- and two-moment schemes, *Mon. Weather Rev.*, *137*, 991–1007, doi:10.1175/2008MWR2556.1.

Olson, W., L. Tian, M. Grecu, K. Kuo, B. Johnson, A. Heymsfield, A. Bansemer, G. Heymsfield, J. Wang, and R. Meneghini (2016), The microwave radiative properties of falling snow derived from nonspherical ice particle models. Part II: Initial testing using radar, radiometer and in situ observations, *J. Appl. Meteorol. Climatol.*, *55*, 709–722, doi:10.1175/JAMC-D-15-0131.1.

Shen, F. F., and J. Z. Min (2015), Assimilating AMSU-A radiance data with the WRF hybrid En3DVAR system for track predictions of Typhoon Megi (2010), *Adv. Atmos. Sci.*, *32*, 1231–1243, doi:10.1007/s00376-014-4239-4.

Skamarock, W. C., J. B. Klemp, J. Dudhia, D. O. Gill, D. M. Barker, M. G. Duda, X.-Y. Huang, W. Wang, and J. G. Powers (2008), A description of the advanced research WRF version 3, *NCAR Tech. Note NCAR/TN-475+STR*.

Surussavadee, C., and D. H. Staelin (2006), Comparison of AMSU millimeter-wave satellite observations, MM5/TBSCAT predicted radiances, and electromagnetic models for hydrometeors, *IEEE Trans. Geosci. Remote Sens.*, *44*, 2667–2678, doi:10.1109/TGRS.2006.873275.

Thompson, G., P. R. Field, R. M. Rasmussen, and W. D. Hall (2008), Explicit forecasts of winter precipitation using an improved bulk microphysics scheme. Part II: Implementation of a new snow parameterization, *Mon. Weather Rev.*, *136*, 5095–5114.

Turner, D. D., S. Kneifel, and M. P. Cadeddu (2016), An improved liquid water absorption model at microwave frequencies for supercooled liquid water clouds, *J. Atmos. Oceanic Technol.*, *33*, 1, doi:10.1175/JTECHD-15-0074.1.

Weng, Y., and F. Zhang (2012), Assimilating airborne Doppler radar observations with an ensemble Kalman filter for cloud-resolving hurricane initialization and prediction: Katrina (2005), *Mon. Weather Rev.*, *140*, 841–859, doi:10.1175/2011MWR3602.1.

Wiedner, M., C. Prigent, J. R. Pardo, O. Nuissier, J.-P. Chaboureau, J.-P. Pinty, and P. Mascart (2004), Modeling of passive microwave responses in convective situations using output from mesoscale models: Comparison with TRMM/TMI satellite observations, *J. Geophys. Res.*, *109*, D06214, doi:10.1029/2003JD004280.

Zhang, F., and Y. Weng (2015), Predicting hurricane intensity and associated hazards: A five-year real-time forecast experiment with assimilation of airborne Doppler radar observations, *Bull. Am. Meteorol. Soc.*, *96*, 25–32.

Zhang, M., M. Zupanski, M.-J. Kim, and J. A. Knaff (2013), Assimilating AMSU-A radiances in the TC core area with NOAA operational HWRF (2011) and a hybrid data assimilation system: Danielle (2010), *Mon. Weather Rev.*, *141*, 3889–3907, doi:10.1175/MWR-D-12-00340.1.

Zhu, T., F. Weng, M. Masutani, and J. S. Woollen (2012), Synthetic radiance simulation and evaluation for a Joint Observing System Simulation Experiment, *J. Geophys. Res.*, *117*, D23111, doi:10.1029/2012JD017697.

Zhu, Y., and R. Gelaro (2008), Observation sensitivity calculations using the adjoint of the Gridpoint Statistical Interpolation (GSI) analysis system, *Mon. Weather Rev.*, *136*, 335–351, doi:10.1175/MWR3525.1.